Unidirectional Giant Exciton Emission into a Photonic Waveguide

Qifa Wang,[1,*] Huan Luo,[1,*] Chaojie Ma,[2,*] Bingchang Zhang,[3] Cheng Ji,[1] Qinghong Yu,[1] Guoxiang Chai,[1] Yuxin Li,[1] Chenyang Li,[1] Shaojun Wang,[3] Xuetao Gan,[1,†] Kaihui Liu,[4,‡] Jianlin Zhao,[1] and Fajun Xiao[1,§]

[1]*Key Laboratory of light-field manipulation and information acquisition, Ministry of Industry and Information Technology, and Shaanxi Key Laboratory of Optical Information Technology, School of Physical Science and Technology, Northwestern Polytechnical University, Xi'an 710129, China*

[2]*Beijing National Laboratory for Condensed Matter Physics, Institute of Physics, Chinese Academy of Sciences, Beijing 100190, China*

[3]*Key Lab of Advanced Optical Manufacturing Technologies of Jiangsu Province, Key Lab of Modern Optical Technologies of Education Ministry of China, School of Optoelectronic Science and Engineering, Soochow University, Suzhou 215006, China*

[4]*State Key Laboratory for Mesoscopic Physics, Collaborative Innovation Centre of Quantum Matter, Frontiers Science Center for Nanooptoelectronics, School of Physics, Peking University, Beijing 100871, China*

(Received 27 May 2025; accepted 5 September 2025; published 1 October 2025)

Efficient coupling of nanolight sources into photonic waveguides is crucial for integrated photonics, quantum technologies, and biosensing. Practical implementations require light sources with simultaneous high brightness and unidirectional emission. However, it is fundamentally incompatible between strong electromagnetic field confinement and directional radiation. Here, we demonstrate the simultaneous giant excitonic photoluminescence (PL) enhancement and unidirectional emission from a two-dimensional InSe film integrated with an asymmetric plasmonic nanocavity. A 3500-fold PL enhancement is achieved by engineering spatial, spectral, and orientational overlap between cavity modes and out-of-plane excitons in InSe. Symmetry breaking within the nanocavity ensures precise control of emission interference, yielding a record-high directivity exceeding 15 dB. The design achieves a high coupling efficiency of 24% and supports guided light propagation of 140 μm. Our results establish a scalable approach for the ultracompact integration of nanoscale light sources into monolithic photonic circuits and will advance the development of on-chip nanophotonics.

DOI: 10.1103/3fxz-6v6s

Two-dimensional (2D) semiconductors, with their exotic optical properties and ultrathin dimensions, hold transformative potential as nanoscale light sources [1–3]. Their unique merits of miniaturized device footprints, low power consumption, and good compatibility offer a versatile platform for advancing integrated photonics [4], quantum technologies [5], bioimaging [6], and biosensing [7]. One crucial step towards the aforementioned applications lies in the efficient coupling of excitonic emission from 2D materials to photonic waveguides. A common approach involves the direct integration of 2D materials atop or beneath waveguides [8,9]. However, this method suffers from limited near-field evanescent coupling efficiency due to the inadequate overlap between waveguide mode and 2D materials. An alternative strategy embeds the 2D material within a slab waveguide, which improves coupling efficiency by aligning the emission with the waveguide modes [10,11]. Nevertheless, the intrinsic omnidirectional emission of 2D materials inevitably introduces the increased loss, uncontrolled light paths, and unwanted interference. Moreover, the inherent thin-film nature of 2D materials leads to weak light absorption [12] and low quantum yield [13], severely limiting the propagation distance and restricting their practical applications.

To address the aforementioned challenges, extensive research endeavors have been dedicated to enhance the emission directionality and intensity of nanoemitters through various nanostructures, including Yagi-Uda antennas [14,15], metasurfaces [16,17], V-shape antenna [18], Mie nanoparticles [19,20], and nanoparticle-on-mirror (NPOM) nanocavity [21,22]. The NPOM nanocavity, composed of a metallic nanoparticle and film with a nanometric gap layer, exhibits unparalleled ability to confine light to an ultrasmall volume [23] with extremely large field enhancement [24]. Benefiting from the bottom-up fabrication procedure, 2D materials can be precisely embedded in the region of maximum intensity within the gap layer [25]. This leads to a significant enhancement in light absorption as well as an acceleration of the emission rate due to the Purcell effect, resulting in orders of magnitude increase in photoluminescence (PL) intensity [26]. Meanwhile, the NPOM nanocavity can function as a

*These authors contributed equally to this work.
†Contact author: xuetaogan@nwpu.edu.cn
‡Contact author: khliu@pku.edu.cn
§Contact author: fjxiao@nwpu.edu.cn

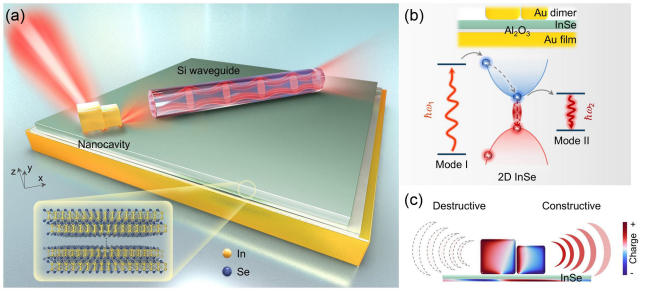

FIG. 1. Asymmetric nanocavity for enhancing and directing excitonic emission into a photonic waveguide. (a) Schematic of the integrated system comprising an Au nanocube dimer-on-mirror nanocavity, a 2D InSe layer, and a Si nanowire waveguide. (b) Energy diagram of PL processes in the InSe-coupled nanocavity, showing absorption ($\hbar\omega_1$) and emission ($\hbar\omega_2$) enhancement mediated by cavity modes I and II, respectively. (c) Interference model illustrating directional emission enabled by symmetry breaking in the nanocavity.

nanopatch antenna to direct emission towards surface normal by using a high radiative dipolar mode [27]. However, this out-of-plane (OP) directional emission is misaligned with the waveguide on the chip, eventually delivering a low coupling efficiency. In fact, in-plane directionality and a large Purcell factor are inherently mutually exclusive. Achieving a high Purcell factor requires an ultrasmall mode volume, which in turn necessitates strong transverse field confinement. This spatial localization corresponds to a broad spectrum in the spatial frequency domain, as dictated by Fourier transform, and consequently restricts directional emission in the far field [28].

To overcome this dilemma, we develop an approach that simultaneously enhances and directionally controls the exciton emission of 2D InSe using an asymmetric nanocavity with an Au nanocube dimer-on-mirror (NDOM) configuration. The delicate control of plasmon hybridization via the symmetry of the dimer enables optimal spatial, spectral, and orientational matching between the plasmonic modes and the OP exciton of InSe, leading to an over 3500-fold enhancement in PL intensity. Meanwhile, the symmetry breaking in the dimer introduces an internal phase retardation across the nanocavity, which enables the emission with a high directionality through constructive and destructive interferences in two opposite directions. Consequently, this nanocavity antenna demonstrates the unidirectional launching of exciton emission into a Si nanowire waveguide, achieving a remarkably high coupling efficiency and a long-guided distance.

The concept of our design is schematically illustrated in Fig. 1(a), where the exciton emission from 2D InSe is enhanced by the asymmetric nanocavity and then directionally routed to a Si nanowire waveguide. To achieve simultaneous enhancement of absorption and quantum yield, the nanocavity is designed to support two spectrally distinct plasmonic modes, which arise from plasmon hybridization within the nanocavity, as illustrated in Fig. S1 of the Supplemental Material [29]. As depicted in the energy diagram [Fig. 1(b)], cavity mode I is energetically aligned with the excitation energy to boost the absorption efficiency. The as-excited electrons and holes subsequently relax into excitons, which then couple to cavity mode II. This mode spectrally overlaps with the exciton emission energy, enhancing the radiative decay rate through the Purcell effect. Furthermore, the symmetry breaking of nanocavity perturbs the charge distribution (see Fig. S2 of the Supplemental Material [29]), which modifies the phase and amplitude of exciton emission. As a result, the originally omnidirectional OP exciton emission is reshaped into a directional pattern via interference, as shown in Fig. 1(c), facilitating efficient coupling into the photonic waveguide.

To validate the design, we perform full-wave electromagnetic simulations of the InSe-coupled nanocavity. The excitation (633 nm) and emission (980 nm) wavelengths of InSe are used as references. Nanocubes with edge lengths of $l_L = 110$ nm and $l_R = 90$ nm are chosen to spectrally align cavity modes I and II with these wavelengths. As shown in Fig. 2(a), the corresponding resonances demonstrate strong field confinement in the nanogap (see Fig. S3 in the Supplemental Material [29]), thereby ensuring a strong plasmon-exciton interaction. The corresponding enhancements in excitation and emission rates are presented in Fig. 2(b). The excitation process, governed by the local electric field $\mathbf{E}$ and the excitonic transition dipole moment $\mathbf{p}$ [52], follows $\gamma_{ex} \propto |\mathbf{p} \cdot \mathbf{E}|^2$. Notably, mode I substantially enhances the OP local field E_z within the gap region, which aligns well with the OP exciton p_z of InSe. This electric field-dipole alignment leads to a pronounced excitation rate enhancement, exceeding a factor of 960 near the nanocube corners [Fig. 2(b), left panel]. On the other hand, the emission rate is determined by the photonic environment, namely, the local density of optical states (LDOS), which scales as $\rho \propto \mathbf{n}_p \cdot \mathrm{Im}\{G(\mathbf{r},\mathbf{r})\} \cdot \mathbf{n}_p$ [26]. Here, $\mathbf{n}_p$ represents the orientation of the transition dipole moment, and $G(\mathbf{r},\mathbf{r})$ refers to the dyadic Green's function at the position $\mathbf{r}$. Mode II compresses the optical field into an ultrasmall mode volume with an orientation matching that of the excitonic dipole, thereby enhancing the LDOS and boosting the emission rate. This leads to a sevenfold enhancement in quantum yield at the emission wavelength compared to bare InSe [Fig. 2(b), right panel].

To elucidate the far-field emission characteristics, mode II is modeled as two coherently oscillating dipoles, $\mathbf{P}_1$ and $\mathbf{P}_2$, laterally separated by a distance d [Fig. 2(c), inset]. The resulting scattering pattern arises from the interference between their radiated fields. Directional radiation is achieved through constructive interference along one direction and destructive interference along the opposite [53].

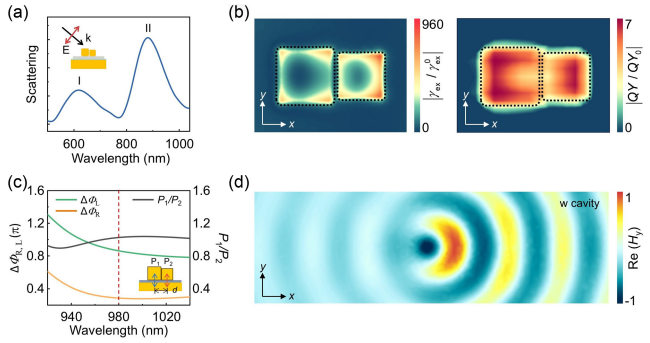

FIG. 2. Simulated PL enhancement and directional emission in a 2D InSe-coupled nanocavity. (a) Simulated scattering spectrum of the InSe-coupled nanocavity. The inset shows the excitation geometry under p-polarized side illumination. (b) Enhancement maps of excitation rate (left) and quantum efficiency (right) within the nanocavity, normalized to those of out-of-plane (OP) excitons in bare InSe. Dashed lines indicate the lateral boundaries of the nanocube dimer. (c) Two-dipole model describing unidirectional radiation from NDOM nanocavity. The green and yellow lines indicate phase differences along the negative (Φ_L) and positive (Φ_R) x directions, respectively, while the gray line shows the relative dipole amplitude (P_1/P_2). (d) Simulated magnetic field (H_y) distribution demonstrating unidirectional emission from the InSe-coupled nanocavity.

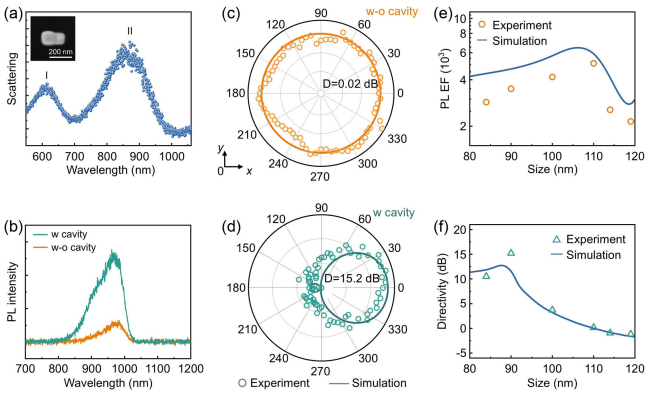

FIG. 3. Experimental demonstration of PL enhancement and directional emission of 2D InSe-coupled nanocavity. (a) Measured scattering spectrum of InSe-coupled nanocavity, exhibiting two distinct resonant modes aligned with the excitation and emission wavelengths of InSe. The inset shows a SEM image of the nanocavity. (b) PL spectra of InSe with (green) and without nanocavity (yellow), revealing pronounced PL enhancement. (c), (d) In-plane angular emission patterns of InSe without (c) and with (d) nanocavity. The dots and solid lines represent the experimental and simulated results, respectively. (e),(f) Dependence of PL enhancement (e) and emission directivity (f) on the dimension of the right nanocube, while the left nanocube dimension is fixed at 110 nm. The dots and solid lines represent the experimental and simulated results, respectively.

Symmetry breaking in the dimer modifies the relative amplitude (P_1/P_2) and phase difference $\Phi_{L,R} = (\Delta\phi \pm kd)$ between the two dipoles. Here, k is the wave vector and $\Delta\phi$ represents the internal phase retardation between two dipoles, which depends on their plasmon resonance condition [54]. Our simulation reveals that an asymmetric nanocavity, with nanocube lengths of $l_L = 110$ nm and $l_R = 90$ nm, functions as a unidirectional antenna. At an emission wavelength of $\lambda = 980$ nm, analysis of the simulated surface charges [see Fig. 1(c) and note 1 of the Supplemental Material [29]] yields $P_1/P_2 = 1.02$ with $\Phi_L = 0.86\pi$ and $\Phi_R = 0.28\pi$. This indicates that the asymmetry results in suppressed radiation in the negative x direction and enhanced radiation in the positive x direction, thereby achieving directional scattering [53]. The coupling between the asymmetric nanocavity antenna and the emitter significantly modifies the emission profile, such that the OP exciton emission is fully governed by the nanocavity antenna [55]. Figure 2(d) shows the simulated emitted magnetic field (H_y) distribution from OP exciton coupled asymmetric nanocavity. A strong preferential propagation along the positive x direction is clearly observed, which exhibits excellent agreement with the theoretical predictions.

The asymmetric nanocavity was fabricated using a bottom-up approach (see Methods of the Supplemental Material [29]). The inset of Fig. 3(a) displays a scanning electron microscope (SEM) image of the resulting nanocavity, revealing a tightly packed nanocube dimer with edge lengths of $l = 110$ and 90 nm. The measured scattering spectrum of the nanocavity [see Fig. 3(a)] exhibits a distinct double-resonance feature, indicating resonant alignment between the cavity modes, the excitation laser, and the exciton emission. PL measurements further confirm this coupling effect. As shown in Fig. 3(b), the PL intensity from InSe monolayers is dramatically enhanced when coupled to the nanocavity, consistent with the simulated results in Fig. 2(b). Specifically, a more than 3500-fold enhancement in PL intensity is observed compared to uncoupled regions (see note 2 of the Supplemental Material [29]).

To resolve the angular distribution of the emitted light, we employed the back focal plane (BFP) imaging technique (see Methods of the Supplemental Material [29]). Figures 3(c) and 3(d) show the polar plots of emission patterns extracted from the BFP images (see Fig. S4 of the Supplemental Material [29]). In the absence of the cavity, the emission exhibits an omnidirectional emission pattern [Fig. 3(c) and Fig. S4(a) of the Supplemental Material [29]], where the ring-shaped distribution, along with its radial polarization (see Fig. S5 of the Supplemental Material [29]), clearly verified the OP dipole emission characteristic [56,57]. In contrast, when coupled with the nanocavity, the emission pattern is significantly reshaped into a single-lobe profile [Fig. 3(d)], indicating a transition to unidirectional emission. This demonstrates the role of the nanocavity in modulating the emission profile through coupling between the OP exciton and the antenna mode of

the cavity. Notably, the measured far-field patterns are in excellent agreement with simulations, as shown by the comparison between experimental data (dots) and numerical results (solid lines) in Figs. 3(c) and 3(d).

To quantify the directionality of emission, we introduce a parameter of directivity D, which is defined as the logarithmic ratio of the emitted power $S(\varphi,\theta)$ in the positive and negative x directions [58]

$$D = 10\log_{10}\frac{\int_{-\theta_{\min}}^{-\theta_{\mathrm{NA}}}\int_{0^\circ-\delta}^{0^\circ+\delta} S(\varphi,\theta)|\sin\theta|\mathrm{d}\varphi\mathrm{d}\theta}{\int_{\theta_{\min}}^{\theta_{\mathrm{NA}}}\int_{180^\circ-\delta}^{180^\circ+\delta} S(\varphi,\theta)|\sin\theta|\mathrm{d}\varphi\mathrm{d}\theta}\mathrm{dB}, \quad (1)$$

where $\theta_{\mathrm{NA}} = 64.2^\circ$ denotes the maximum collection angle of the objective, $\theta_{\min} = 34.2^\circ$ is the minimum polar angle for the waveguide collection, and $\delta = 45^\circ$ corresponds to azimuthal collection half angle. According to Eq. (1), the emission directivity D in Fig. 3(d) is determined to be 15.2 dB, which surpasses previously reported values for emitter-coupled nanoantennas (see Table S1 of the Supplemental Material [29]), while maintaining an ultracompact footprint of $\sim 0.02\lambda^2$. Furthermore, systematic measurements on 5 nearly identical nanocavities ($l_{\mathrm{L}} = 110$ and $l_R = 90$ nm) yield an average directivity of 15.2 ± 0.9 dB and a PL enhancement factor of 3497 ± 165, confirming a good reproducibility (see Fig. S6 of the Supplemental Material [29]).

In the following, we examine the influence of nanocavity symmetry on the PL enhancement and emission directivity, as shown in Figs. 3(e) and 3(f). The symmetry is tuned by varying the right nanocube size form $l_R = 80$ to 120 nm, while keeping the left nanocube fixed at $l_L = 110$ nm. Both the PL enhancement factor and emission directivity initially increase and then decrease with increasing l_{R}, showing peak responses at $l_{\mathrm{R}} = 110$ and 90 nm, respectively. The offset in optimal l_{R} reflects distinct physical origins: PL enhancement maximizes when the geometry of cavity balances excitation rate and quantum yield, while directivity peaks when the interference contrast between two symmetry-controlled dipoles is largest. Numerical simulations reproduce these trends and support this interpretation (see Supplemental Material [29], Figs. S7 and S8 for more details).

To demonstrate the directional coupling, a Si nanowire waveguide with a diameter of 320 nm was positioned in close proximity to the asymmetric nanocavity (see Methods of the Supplemental Material [29]), as shown in Fig. 4(a). Facilitated by the asymmetric nanocavity antenna, a substantial portion of OP exciton emission is funneled into the waveguide. This is evidenced by simulations of the magnetic field distribution (H_{y}) shown in Fig. 4(b), which reveal efficient coupling into the waveguide's fundamental TM_0 mode with the field tightly confined within the core. Experimentally, directional coupling is confirmed by the PL images obtained under horizontally polarized excitation [Fig. 4(c)]. In the top panel, the strong signal from the left

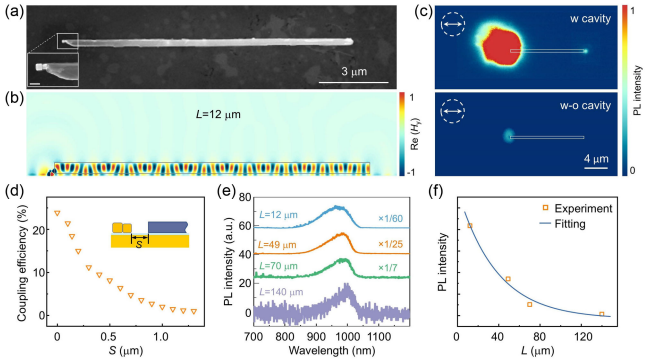

FIG. 4. Unidirectional coupling of exciton emission into a photonic waveguide via an asymmetric nanocavity. (a) SEM image of the integrated system comprising an asymmetric nanocavity and a Si nanowire waveguide. The inset shows a magnified view, demonstrating the precise alignment between the nanocavity and the waveguide (scale bar: 200 nm). (b) Simulated emission profile from an OP dipole source positioned beneath the nanocube dimer, demonstrating directional coupling into the waveguide. (c) PL maps of the integrated system (top) and the bare Si waveguide (bottom) under horizontally polarized excitation. (d) Coupling efficiency between the OP dipolar emitter and the Si waveguide as a function of dimer-waveguide separation at the emission wavelength ($\lambda_{\mathrm{em}} = 980$ nm). (e) PL spectra measured at the distal end of the waveguides with varying lengths. (f) PL peak intensity at the distal end versus the waveguide length, with experimental data (points) fitted by an exponential decay (line).

spot originates directly from the asymmetric nanocavity, whereas the spot on the right corresponds to the outcoupled light at the distal end of the waveguide. By contrast, in the absence of the nanocavity [Fig. 4(c), bottom panel], the PL signal from the left side of the waveguide diminishes by a factor of 4.6, accompanied by the disappearance of distal emission. This demonstrates the role of the asymmetric nanocavity in enhancing and directing the exciton emission from InSe.

Quantitatively, the coupling efficiency, defined as the ratio of guided mode power to total OP exciton emission, was extracted from simulations [Fig. 4(d)]. The coupling efficiency increases as the separation S between the nanocavity and waveguide decreases, reaching up to 24% when the structures are assembled using our nanomanipulation technique [Fig. 4(a)]. Figure 4(e) presents the PL spectra collected at the waveguide output for various lengths. A guided distance of up to 140 μm is achieved due to the large emission enhancement and coupling efficiency enabled by the directional nanocavity antenna. The peak PL intensities exhibit an exponential decay with increasing waveguide length, yielding an attenuation coefficient of 0.026 $\mu\mathrm{m}^{-1}$, as shown in Fig. 4(f). This loss is primarily attributed to self-absorption in the InSe layer and Ohmic loss of Au substrate, which could be mitigated by employing low-loss dielectric materials beyond the cavity region.

In summary, we have demonstrated the directional coupling of exciton emission from 2D InSe to a Si nanowire waveguide through an asymmetric plasmonic nanocavity. Our design effectively addresses the fundamental incompatibility between strong field confinement and narrow angular emission, which is constrained by the Fourier transform limit. The asymmetric nanocavity serves as an efficient directional coupler, guiding the exciton emission toward the Si waveguide with high coupling efficiency and extended guided distance. Owing to its material and spectral flexibility, the platform can integrate with a wide range of quantum emitters, including other 2D semiconductors and colloidal quantum dots. This integration offers a promising route toward deterministic waveguide coupling of single-photon sources, facilitating the development of scalable quantum photonic integrated circuits for applications in information processing, sensing, and secure communication. By utilizing high-quantum-yield gain materials, such as perovskite quantum dots, the same structure can function as a low-threshold on-chip nanolaser under optical pumping [59]. Additionally, its particle-on-mirror geometry allows for quantum tunneling-based electrical excitation, paving the way for compact, and electrically driven nanolight sources [60]. The design is also compatible with large-scale fabrication using either top-down lithography [61] or bottom-up self-assembly techniques [62], which can be used to fabricate arrays of directional emitters. When combined with other photonic components, such as plasmonic waveguides, these emitter arrays can serve as active, ultracompact, and multifunctional building blocks for next-generation integrated nanophotonic systems.

Acknowledgments—This work was supported by the National Key R&D Program of China (No. 2022YFA1404800), National Natural Science Foundation of China (NSFC) (No. 52025023, No. 12274345, No. 62275184, and No. 62411540033), Natural Science Basic Research Plan in Shaanxi Province (No. 2024JC-JCQN-08), Innovation Foundation for Doctor Dissertation of Northwestern Polytechnical University (No. CX2022078), Analytical & Testing Center of Northwestern Polytechnical University (No. 2023T022).

Data availability—The data that support the findings of this article are not publicly available. The data are available from the authors upon reasonable request.

[1] Y. Ye, Z. J. Wong, X. Lu, X. Ni, H. Zhu, X. Chen, Y. Wang, and X. Zhang, Monolayer excitonic laser, Nat. Photonics **9**, 733 (2015).

[2] K. Parto, S. I. Azzam, K. Banerjee, and G. Moody, Defect and strain engineering of monolayer WSe_2 enables site-controlled single-photon emission up to 150 K, Nat. Commun. **12**, 3585 (2021).

[3] W. Meng *et al.*, Three-dimensional monolithic micro-LED display driven by atomically thin transistor matrix, Nat. Nanotechnol. **16**, 1231 (2021).

[4] Y. Bie *et al.*, A $MoTe_2$-based light-emitting diode and photodetector for silicon photonic integrated circuits, Nat. Nanotechnol. **12**, 1124 (2017).

[5] F. Peyskens, C. Chakraborty, M. Muneeb, D. Van Thourhout, and D. Englund, Integration of single photon emitters in 2D layered materials with a silicon nitride photonic chip, Nat. Commun. **10**, 4435 (2019).

[6] T. Liu *et al.*, Iron oxide decorated MoS_2 nanosheets with double PEGylation for chelator-free radiolabeling and multimodal imaging guided photothermal therapy, ACS Nano **9**, 950 (2015).

[7] P. T. K. Loan, W. Zhang, C. Lin, K. Wei, L. Li, and C. Chen, Graphene/MoS_2 heterostructures for ultrasensitive detection of DNA hybridisation, Adv. Mater. **26**, 4838 (2014).

[8] H. Chen, V. Corboliou, A. S. Solntsev, D. Y. Choi, M. A. Vincenti, D. De Ceglia, C. De Angelis, Y. Lu, and D. N. Neshev, Enhanced second-harmonic generation from two-dimensional $MoSe_2$ on a silicon waveguide, Light Sci. Appl. **6**, e17060 (2017).

[9] X. Liu *et al.*, Coupling of photon emitters in monolayer WS_2 with a photonic waveguide based on bound states in the continuum, Nano Lett. **23**, 3209 (2023).

[10] S. W. LaGasse *et al.*, Hexagonal boron nitride slab waveguides for enhanced spectroscopy of encapsulated 2D materials, Adv. Mater. **36**, 2309777 (2024).

[11] R. Khelifa, S. Shan, A. J. Moilanen, T. Taniguchi, K. Watanabe, and L. Novotny, WSe_2 light-emitting device coupled to an h-BN waveguide, ACS Photonics **10**, 1328 (2023).

[12] K. F. Mak, K. He, C. Lee, G. H. Lee, J. Hone, T. F. Heinz, and J. Shan, Tightly bound trions in monolayer MoS_2, Nat. Mater. **12**, 207 (2013).

[13] K. F. Mak, C. Lee, J. Hone, J. Shan, and T. F. Heinz, Atomically thin MoS_2: A new direct-gap semiconductor, Phys. Rev. Lett. **105**, 136805 (2010).

[14] A. G. Curto, G. Volpe, T. H. Taminiau, M. P. Kreuzer, R. Quidant, and N. F. van Hulst, Unidirectional emission of a quantum dot coupled to a nanoantenna, Science **329**, 930 (2010).

[15] T. Kosako, Y. Kadoya, and H. F. Hofmann, Directional control of light by a nano-optical Yagi-Uda antenna, Nat. Photonics **4**, 312 (2010).

[16] K. Rong, B. Wang, A. Reuven, E. Maguid, B. Cohn, V. Kleiner, S. Katznelson, E. Koren, and E. Hasman, Photonic Rashba effect from quantum emitters mediated by a Berry-phase defective photonic crystal, Nat. Nanotechnol. **15**, 927 (2020).

[17] Y. Wang, D. Huang, M. Xia, J. Zhou, Y. Chen, Y. Liao, and X. Zhang, Directional chiral exciton emission via topological polarization singularities in all van der Waals metasurfaces, Adv. Mater. **37**, 2414174 (2025).

[18] T. Wen, W. Zhang, S. Liu, A. Hu, J. Zhao, Y. Ye, Y. Chen, C.-W. Qiu, Q. Gong, and G. Lu, Steering valley-polarized emission of monolayer MoS_2 sandwiched in plasmonic antennas, Sci. Adv. **6**, eaao0019 (2020).

[19] J. Fang *et al.*, Directional modulation of exciton emission using single dielectric nanospheres, Adv. Mater. **33**, 2007236 (2021).

[20] A. F. Cihan, A. G. Curto, S. Raza, P. G. Kik, and M. L. Brongersma, Silicon Mie resonators for highly directional light emission from monolayer MoS_2, Nat. Photonics **12**, 284 (2018).
[21] X. Bao *et al.*, Giant out-of-plane exciton emission enhancement in two-dimensional indium selenide via a plasmonic nanocavity, Nano Lett. **23**, 3716 (2023).
[22] Z. Lu, J. Ji, H. Ye, H. Zhang, S. Zhang, and H. Xu, Quantifying the ultimate limit of plasmonic near-field enhancement, Nat. Commun. **15**, 8803 (2024).
[23] F. Benz *et al.*, Single-molecule optomechanics in "picocavities," Science **354**, 726 (2016).
[24] C. Ciracì, R. Hill, J. Mock, Y. Urzhumov, A. Fernández-Domínguez, S. Maier, J. Pendry, A. Chilkoti, and D. Smith, Probing the ultimate limits of plasmonic enhancement, Science **337**, 1072 (2012).
[25] B. Wen *et al.*, Manipulating the light-matter interactions in plasmonic nanocavities at 1 nm spatial resolution, Light Sci. Appl. **11**, 235 (2022).
[26] G. M. Akselrod, C. Argyropoulos, T. B. Hoang, C. Ciraci, C. Fang, J. Huang, D. R. Smith, and M. H. Mikkelsen, Probing the mechanisms of large Purcell enhancement in plasmonic nanoantennas, Nat. Photonics **8**, 835 (2014).
[27] C. Li, H. Luo, L. Hou, Q. Wang, K. Liu, X. Gan, J. Zhao, and F. Xiao, Giant photoluminescence enhancement of monolayer WSe_2 using a plasmonic nanocavity with on-demand resonance, Nano Lett. **24**, 5879 (2024).
[28] H. Abudayyeh, A. Mildner, D. Liran, B. Lubotzky, L. Luder, M. Fleischer, and R. Rapaport, Overcoming the rate-directionality trade-off: A room-temperature ultrabright quantum light source, ACS Nano **15**, 17384 (2021).
[29] See Supplemental Material at http://link.aps.org/supplemental/10.1103/3fxz-6v6s for additional details, which includes Refs. [30–51].
[30] G. M. Akselrod, T. Ming, C. Argyropoulos, T. B. Hoang, Y. Lin, X. Ling, D. R. Smith, J. Kong, and M. H. Mikkelsen, Leveraging nanocavity harmonics for control of optical processes in 2D semiconductors, Nano Lett. **15**, 3578 (2015).
[31] Q. Wang, J. Liu, C. Li, L. Hou, P. Wang, X. Gan, K. Liu, D. Lei, J. Zhao, and F. Xiao, On-demand fabrication and manipulation of single plasmonic trimers for ultrasensitive enantiomer detection, Adv. Funct. Mater. **35**, 2412985 (2025).
[32] C. Li, Q. Wang, R. Yi, X. Zhang, X. Gan, K. Liu, J. Zhao, and F. Xiao, Room-temperature two-dimensional InSe plasmonic laser, Nano Lett. **24**, 12935 (2024).
[33] P. B. Johnson and R. W. Christy, Optical constants of the noble metals, Phys. Rev. B **6**, 4370 (1972).
[34] C. Schinke *et al.*, Uncertainty analysis for the coefficient of band-to-band absorption of crystalline silicon, AIP Adv. **5**, 067168 (2015).
[35] Y. Lu, H. Yu, Y. Wang, C. Hung, Y. Chen, J. Jhou, P. T. Yen, J. Hsu, and R. Sankar, Optical determination of layered-materials InSe thickness via RGB contrast method and regression analysis, Nanotechnology **33**, 485702 (2022).
[36] S. Lei *et al.*, Evolution of the electronic band structure and efficient photo-detection in atomic layers of InSe, ACS Nano **8**, 1263 (2014).
[37] H. Kuwata, H. Tamaru, K. Esumi, and K. Miyano, Resonant light scattering from metal nanoparticles: Practical analysis beyond Rayleigh approximation, Appl. Phys. Lett. **83**, 4625 (2003).
[38] T. Coenen, E. J. R. Vesseur, A. Polman, and A. F. Koenderink, Directional emission from plasmonic Yagi-Uda antennas probed by angle-resolved cathodoluminescence spectroscopy, Nano Lett. **11**, 3779 (2011).
[39] M. S. Eggleston and M. C. Wu, Efficient coupling of an antenna-enhanced nanoLED into an integrated InP waveguide, Nano Lett. **15**, 3329 (2015).
[40] J. Ho, Y. H. Fu, Z. Dong, R. Paniagua-Dominguez, E. H. H. Koay, Y. F. Yu, V. Valuckas, A. I. Kuznetsov, and J. K. W. Yang, Highly directive hybrid metal-dielectric Yagi-Uda nanoantennas, ACS Nano **12**, 8616 (2018).
[41] K. See, F. Lin, T. Chen, Y. Huang, C. Huang, A. T. M. Yesilyurt, and J. Huang, Photoluminescence-driven broadband transmitting directional optical nanoantennas, Nano Lett. **18**, 6002 (2018).
[42] R. Kullock, M. Ochs, P. Grimm, M. Emmerling, and B. Hecht, Electrically-driven Yagi-Uda antennas for light, Nat. Commun. **11**, 115 (2020).
[43] D. Vercruysse, X. Zheng, Y. Sonnefraud, N. Verellen, G. D. Martino, L. Lagae, G. A. E. Vandenbosch, V. V. Moshchalkov, S. A. Maier, and P. V. Dorpe, Directional fluorescence emission by individual V-antennas explained by mode expansion, ACS Nano **8**, 8232 (2014).
[44] A. Dasgupta, D. Singh, R. P. N. Tripathi, and G. V. P. Kumar, Directional fluorescence emission mediated by chemically-prepared plasmonic nanowire junctions, J. Phys. Chem. C **120**, 17692 (2016).
[45] S. P. Gurunarayanan, N. Verellen, V. S. Zharinov, F. J. Shirley, V. V. Moshchalkov, M. Heyns, J. Van de Vondel, I. P. Radu, and P. Van, Dorpe, Electrically driven unidirectional optical nanoantennas, Nano Lett. **17**, 7433 (2017).
[46] I. M. Hancu, A. G. Curto, M. Castro-Lopez, M. Kuttge, and N. F. van Hulst, Multipolar interference for directed light emission, Nano Lett. **14**, 166 (2014).
[47] T. Coenen, F. B. Arango, A. F. Koenderink, and A. Polman, Directional emission from a single plasmonic scatterer, Nat. Commun. **5**, 3250 (2014).
[48] H. Shen, R. Y. Chou, Y. Hui, Y. He, Y. Cheng, H. Chang, L. Tong, Q. Gong, and G. Lu, Directional fluorescence emission from a compact plasmonic-diamond hybrid nanostructure, Laser Photonics Rev. **10**, 647 (2016).
[49] F. Zhu, M. Sanz-Paz, A. I. Fernandez-Dominguez, X. Zhuo, L. M. Liz-Marzan, F. D. Stefani, M. Pilo-Pais, and G. P. Acuna, DNA-templated ultracompact optical antennas for unidirectional single-molecule emission, Nano Lett. **22**, 6402 (2022).
[50] A. T. M. Yesilyurt, M. Sanz-Paz, F. Zhu, X. Wu, K. S. Sunil, G. P. Acuna, and J. S. Huang, Unidirectional meta-emitters based on the Kerker condition assembled by DNA origami, ACS Nano **17**, 19189 (2023).
[51] M. Peter, A. Hildebrandt, C. Schlickriede, K. Gharib, T. Zentgraf, J. Foerstner, and S. Linden, Directional emission from dielectric leaky-wave nanoantennas, Nano Lett. **17**, 4178 (2017).
[52] C. Ciracì, A. Rose, C. Argyropoulos, and D. R. Smith, Numerical studies of the modification of photodynamic

processes by film-coupled plasmonic nanoparticles, J. Opt. Soc. Am. B **31**, 2601 (2014).
[53] D. Vercruysse, Y. Sonnefraud, N. Verellen, F. B. Fuchs, G. Di Martino, L. Lagae, V. V. Moshchalkov, S. A. Maier, and P. Van Dorpe, Unidirectional side scattering of light by a single-element nanoantenna, Nano Lett. **13**, 3843 (2013).
[54] T. Shegai, S. Chen, V. D. Miljkovic, G. Zengin, P. Johansson, and M. Kall, A bimetallic nanoantenna for directional colour routing, Nat. Commun. **2**, 481 (2011).
[55] Y. Meng *et al.*, Bright single-nanocrystal upconversion at sub 0.5 $W\,cm^{-2}$ irradiance via coupling to single nanocavity mode, Nat. Photonics **17**, 73 (2023).
[56] M. Brotons-Gisbert, R. Proux, R. Picard, D. Andres-Penares, A. Branny, A. Molina-Sánchez, J. F. Sánchez-Royo, and B. D. Gerardot, Out-of-plane orientation of luminescent excitons in two-dimensional indium selenide, Nat. Commun. **10**, 3913 (2019).
[57] C. Li *et al.*, Room-temperature near-infrared excitonic lasing from mechanically exfoliated InSe microflake, ACS Nano **16**, 1477 (2021).
[58] T. Pakizeh and M. Kall, Unidirectional ultracompact optical nanoantennas, Nano Lett. **9**, 2343 (2009).
[59] Y. H. Hsieh, B. W. Hsu, K. N. Peng, K. W. Lee, C. W. Chu, S. W. Chang, H. W. Lin, T. J. Yen, and Y. J. Lu, Perovskite quantum dot lasing in a gap-plasmon nanocavity with ultralow threshold, ACS Nano **14**, 11670 (2020).
[60] J. Zheng *et al.*, Active control of excitonic strong coupling and electroluminescence in electrically driven plasmonic nanocavities, Sci. Adv. **11**, eadt9808 (2025).
[61] L. Zheng *et al.*, Deep subwavelength control of valley polarized cathodoluminescence in h-BN/WSe_2/h-BN heterostructure, Nat. Commun. **12**, 291 (2021).
[62] S. Ye, H. Zha, Y. Xia, W. Dong, F. Yang, C. Yi, J. Tao, X. Shen, D. Yang, and Z. Nie, Centimeter-scale superlattices of three-dimensionally orientated plasmonic dimers with highly tunable collective properties, ACS Nano **16**, 4609 (2022).